IEEE Access
Multidisciplinary ⋮ Rapid Review ⋮ Open Access Journal

Received February 10, 2020, accepted March 2, 2020, date of publication March 5, 2020, date of current version March 17, 2020.

Digital Object Identifier 10.1109/ACCESS.2020.2978660

Simple Chaotic Jerk Flows With Families of Self-Excited and Hidden Attractors: Free Control of Amplitude, Frequency, and Polarity

IRFAN AHMAD AND BANLUE SRISUCHINWONG
Sirindhorn International Institute of Technology, Thammasat University, Pathum Thani 12000, Thailand

Corresponding author: Banlue Srisuchinwong (banlue@siit.tu.ac.th)

This work was supported in part by the Office of the Higher Education Commission, Thailand, through the National Research University Project.

ABSTRACT Although chaotic systems with self-excited and hidden attractors have been discovered recently, there are few investigations about relationships among them. In this paper, using a systematic exhaustive computer search, three elementary three-dimensional (3D) dissipative chaotic jerk flows are proposed with the unique feature of exhibiting different families of self-excited and hidden attractors. These systems have a variable equilibrium for different values of the single control parameter. In the family of self-excited attractors, these systems can have a single all-zero-eigenvalue non-hyperbolic equilibrium or two symmetrical hyperbolic equilibria. Besides, for a particular value of the parameter, these systems have no equilibria, and therefore all the attractors are readily hidden. The proposed systems represent a rare class of chaotic systems in which a single system exhibits three different types of equilibria for different values of the single control parameter. In particular, for a single all-zero-eigenvalue non-hyperbolic equilibrium, the coefficient of the two linear terms provides a simple means to rescale the amplitude and frequency, while the introduction of a new constant in the variable x provides a polarity control. Therefore, a free-controlled chaotic signal can be obtained with the desired amplitude, frequency, and polarity. When implemented as an electronic circuit, the corresponding chaotic signal can be controlled by two independent potentiometers and an adjustable DC voltage source, which is convenient for constructing a chaos-based application system.

INDEX TERMS Amplitude control, chaos, equilibrium, hidden attractor, jerk system, polarity control, self-excited attractor.

I. INTRODUCTION

A three-dimensional (3D) chaotic system is expressed by a set of three coupled first-order ODEs, e.g., [1], whereas a chaotic jerk system is expressed by a single third-order ODE of the form $\dddot{x} = f(x, \dot{x}, \ddot{x})$ [2]. Jerk systems have been of interest because of their simplicity [3], rich dynamics [4], and many engineering applications, e.g., mechanisms for intermittent motion [5] and robotic arms [6].

On the one hand, most familiar examples of 3D chaotic systems, e.g., [1], [7], or jerk systems, e.g., [4], [8] have hyperbolic equilibria, of which all eigenvalues have non-zero real parts [9]. Chaos in a hyperbolic-equilibrium system can be verified by the Shilnikov criterion [10], with a slight extension [11]. On the other hand, several examples of 3D chaotic systems, e.g., [12], or jerk systems, e.g., [13]–[15] have non-hyperbolic equilibria, of which at least one eigenvalue has a zero real part [13]. Such chaotic systems can have neither homoclinic nor heteroclinic orbits [16], and thus chaos cannot be verified by the Shilnikov theorem [10]. Relatively few examples of chaotic systems, particularly chaotic jerk systems, have been reported with an all-zero-eigenvalue non-hyperbolic equilibrium [13], [17]. A nonlinear analysis is required to determine the stability of non-hyperbolic-equilibrium systems, of which the eigenvalues do not have a positive real part [13].

Since the discovery of a hidden attractor in 2010 [18], attractors have been separated into self-excited and hidden attractors [19]. A self-excited attractor has its basin of attraction that intersects with the neighborhood of an equilibrium, whereas a hidden attractor has its basin of attraction that does not [20]. Hidden attractors account for the difficulty of

The associate editor coordinating the review of this manuscript and approving it for publication was Ludovico Minati.

finding them since there is no way to choose initial conditions except by an analytical-numerical algorithm [18]–[20], or by an extensive numerical search [21], [22].

Studies of hidden attractors allow the understanding of potentially unexpected disastrous responses of dynamical systems to perturbations. Such systems include, for example, aircraft control systems [23], a model of drilling systems [24], and convective fluid motion [20]. Consequently, there has been an increasing interest in hidden attractors of chaotic systems, such as systems with no equilibria [25], with surfaces of equilibria [26], with a curve of equilibria [27], and with a stable equilibrium [28].

Recently, both techniques of amplitude-frequency control [17], [29], and polarity control [30], [31], which are known collectively as free control, have been suggested to provide simple and continuous adjustment of chaotic signals without encountering undesirable bifurcations [32], [33]. Both techniques are useful in practical applications, e.g., chaos-based secure communications [34], to reduce the required hardware [31] and to give a desired chaotic signal with the particular requirements of amplitude, frequency, and polarity [35], [36].

Chaotic systems with invariable Lyapunov exponents (LEs) have the property of amplitude control (AC) [37], where the AC can rely on a single circuit component rather than a complicated circuit. Chaotic systems with a single non-quadratic term [17], [29] have an inherent amplitude-frequency controller (AFC) in either a constant non-quadratic term, or a coefficient of a non-quadratic linear term. Some chaotic systems provide polarity control (PC) by the introduction of a new constant in any of the governing equations [30], [31]. The techniques have, however, never been employed for a jerk system that exhibits different families of self-excited and hidden attractors using a single control parameter.

Most existing chaotic jerk systems have a hyperbolic equilibrium, e.g., [2], a non-hyperbolic equilibrium, e.g., [13], or no equilibria, e.g., [38] for different families of self-excited and hidden attractors. In all these systems, different systems exhibit different types of equilibria and attractors. Recently, examples of chaotic systems using adjustable parameters have been reported for different families of self-excited and hidden attractors [39]–[44], whereas only two examples [43], [44] of chaotic jerk systems using adjustable parameters have been demonstrated for different families of self-excited and hidden attractors.

Both existing jerk systems [43], [44] for different families of self-excited and hidden attractors do not provide free control of amplitude, frequency, and polarity. Although the chaotic jerk system in [43] exhibits a non-hyperbolic equilibrium, the system in [44] does not, but [44] exhibits only hyperbolic equilibria or no equilibria. It is natural to wonder whether there exists a chaotic jerk system with different families of self-excited and hidden attractors in which free control of amplitude, frequency, and polarity of chaotic signals is possible.

In this paper, three simple chaotic jerk systems are proposed mostly with quadratic terms of nonlinearity for different families of self-excited and hidden attractors using a single control parameter. The single control parameter performs as a constant controller to select the required dynamics. These systems can have a self-excited chaotic attractor with an all-zero-eigenvalue non-hyperbolic equilibrium, a self-excited chaotic attractor with two symmetrical hyperbolic equilibria, and a hidden chaotic attractor with no equilibria. For the single all-zero-eigenvalue non-hyperbolic equilibrium, the coefficient of the two linear terms provides both amplitude and frequency control, while the introduction of a new constant in the variable x provides polarity control. Therefore, a free controlled chaotic signal can be obtained, with the particular requirements of the amplitude, frequency, and polarity. That means the systems proposed here can provide a full self-modulation of AFC and PC [35].

II. SIMPLE CHAOTIC JERK FLOWS WITH FAMILIES OF SELF-EXCITED AND HIDDEN ATTRACTORS

A. SIMPLE CHAOTIC JERK FLOWS WITH A VARIABLE EQUILIBRIUM

In searching for chaotic jerk systems with a variable equilibrium for different families of self-excited and hidden attractors, a simple general structure of a chaotic jerk system based on quadratic terms of nonlinearity is designed as

$$\begin{cases} \dot{x} = y \\ \dot{y} = z \\ \dot{z} = a_1x^2 + a_2y^2 + a_3z^2 + a_4xy + a_5xz \\ \qquad\quad + a_6yz + a_7 \end{cases} \tag{1}$$

For the parameter $a_1 \neq 0$, the system in (1) has an equilibrium at $E(\pm\sqrt{-a_7/a_1}, 0, 0)$. Let the parameter $a_1 > 0$, the single parameter a_7 behaves as a controller for diverse dynamics in (1), such as dynamics with self-excited and hidden attractors. Depending on the values of a_7, three different types of equilibria can be possible as follows:

Case 1: if $a_7 = 0$, the system in (1) will have a single equilibrium at the origin $E_0 = (0, 0, 0)$. Using the Jacobian of (1), three eigenvalues evaluated at E_0 are $\lambda_{1,2,3} = 0$. As all eigenvalues are zero, E_0 is therefore an all-zero-eigenvalue non-hyperbolic equilibrium.

Case 2: if $a_7 < 0$, the system in (1) will have two symmetrical equilibria at $E_{1,2} = \left(\pm\sqrt{a_7/a_1}, 0, 0\right)$. Using the Jacobian of (1), three eigenvalues evaluated at $E_1 = \left(+\sqrt{a_7/a_1}, 0, 0\right)$ are of the form $\lambda_1^+ = +\alpha$, $\lambda_{2,3}^+ = -\beta \pm j\gamma$; whereas three eigenvalues evaluated at $E_2 = \left(-\sqrt{a_7/a_1}, 0, 0\right)$ are of the form $\lambda_1^- = -\alpha$, $\lambda_{2,3}^- = +\beta \pm j\gamma$; where α, β, γ are non-zero. As the real parts of the eigenvalues are non-zero, both $E_{1,2}$ are therefore hyperbolic equilibria.

Case 3: if $a_7 > 0$, the system in (1) will have no equilibria.

As a result, the chaotic jerk system in (1) belongs to three different families: (*i*) a family of self-excited attractors with an all-zero-eigenvalue non-hyperbolic equilibrium, as described by Case 1, (*ii*) a family of self-excited attractors

TABLE 1. Three simple chaotic jerk flows with different families of self-excited and hidden attractors.

Chaotic Jerk Systems	Equations	Parameters		Equilibria	Types of Equilibria	Types of Attractors
		(a, b)	c	$E\ (x, y, z)$		
VE_1	$\dot{x} = y$ $\dot{y} = z$ $\dot{z} = ax^2 - by^2 + 0.6xz + 0.4yz + c$	$a = 1.0$ $b = 0.9$	$c = 0$ $c = -0.2$ $c = 0.24$	$(0, 0, 0)$ $(\pm\sqrt{-c/a}, 0, 0)$ –	Non-Hyperbolic Hyperbolic No-equilibria	Self-Excited Self-Excited Hidden
VE_2	$\dot{x} = y$ $\dot{y} = z$ $\dot{z} = ax^2 - by^2 + 0.5xy + 0.3xz + c$	$a = 0.5$ $b = 0.6$	$c = 0$ $c = -0.1$ $c = 0.03$	$(0, 0, 0)$ $(\pm\sqrt{-c/a}, 0, 0)$ –	Non-Hyperbolic Hyperbolic No-equilibria	Self-Excited Self-Excited Hidden
VE_3	$\dot{x} = y$ $\dot{y} = z$ $\dot{z} = ax^2 - bz^2 + 0.7xy + 0.3xz + c$	$a = 0.4$ $b = 0.2$	$c = 0$ $c = -0.01$ $c = 0.04$	$(0, 0, 0)$ $(\pm\sqrt{-c/a}, 0, 0)$ –	Non-Hyperbolic Hyperbolic No-equilibria	Self-Excited Self-Excited Hidden

TABLE 2. Eigenvalues, Lyapunov exponents, and Lyapunov dimensions for the three chaotic jerk systems in Table 1.

Chaotic Jerk Systems	Eigenvalues	LEs and D_L			Initial conditions
		Non-hyperbolic	Hyperbolic	No equilibria	(x_0, y_0, z_0)
VE_1	$\lambda_{1,2,3} = 0$ $\lambda_1^+ = 1.0617, \quad \lambda_{2,3}^+ = -0.3967 \pm 0.8277i$ $\lambda_1^- = -1.0617, \quad \lambda_{2,3}^- = 0.3967 \pm 0.8277i$ –	$L_1 = 0.1329$ $L_2 = 0.0000$ $L_3 = -7.4292$ $D_L = 2.0179$	$L_1 = 0.1320$ $L_2 = 0.0000$ $L_3 = -7.4280$ $D_L = 2.0178$	$L_1 = 0.1410$ $L_2 = 0.0000$ $L_3 = -7.3831$ $D_L = 2.0191$	0.1 0.6 −0.8
VE_2	$\lambda_{1,2,3} = 0$ $\lambda_1^+ = 0.9141, \quad \lambda_{2,3}^+ = -0.3899 \pm 0.5807i$ $\lambda_1^- = -0.7078, \quad \lambda_{2,3}^- = 0.2873 \pm 0.7405i$ –	$L_1 = 0.0900$ $L_2 = 0.0000$ $L_3 = -1.3697$ $D_L = 2.0657$	$L_1 = 0.0885$ $L_2 = 0.0000$ $L_3 = -1.3744$ $D_L = 2.0644$	$L_1 = 0.0907$ $L_2 = 0.0000$ $L_3 = -1.3664$ $D_L = 2.0664$	−2.1 0.1 −7
VE_3	$\lambda_{1,2,3} = 0$ $\lambda_1^+ = 0.5933, \quad \lambda_{2,3}^+ = -0.2729 \pm 0.3724i$ $\lambda_1^- = -0.4427, \quad \lambda_{2,3}^- = 0.1977 \pm 0.4966i$ –	$L_1 = 0.0400$ $L_2 = 0.0000$ $L_3 = -1.5621$ $D_L = 2.0256$	$L_1 = 0.0303$ $L_2 = 0.0000$ $L_3 = -1.5569$ $D_L = 2.0194$	$L_1 = 0.0489$ $L_2 = 0.0000$ $L_3 = -1.5480$ $D_L = 2.0316$	−2.6 0 −7

with hyperbolic equilibria, as described by Case 2, and (*iii*) a family of hidden attractors with no equilibria, as described by Case 3. The single control parameter a_7 therefore exhibits a unique characteristic, as three such families in three cases switch from one type of attractors and equilibria to another.

B. AN EXHAUSTIVE SEARCH FOR CHAOS

An exhaustive computer search is performed subject to the constraints on the aforementioned Cases 1, 2, and 3. The exhaustive computer search is based on existing procedures well described by [45] and employs software written and used by permission of the author of [45]. In such procedures, thousands of combinations of coefficients a_1 to a_7 and initial conditions are scanned to find for a positive LE (>0.001), which is a signature of chaos.

For each positive LE (>0.001) being found, the space of the coefficients is searched for values that are deemed elegant simplicity [45], by which as many coefficients as possible are set to zero with the others set to ±1 if possible, or otherwise set to a small integer or a decimal fraction with the fewest possible digits.

Although several chaotic jerk systems are found, only the systems with elegant simplicity are selected, as reported in Table 1. This has identified most of the elementary chaotic jerk systems with quadratic terms, which enable three different families of self-excited and hidden attractors in three different types of equilibria, i.e., a single all-zero-eigenvalue non-hyperbolic equilibrium, two symmetrical hyperbolic equilibria, and no equilibria.

III. NUMERICAL RESULTS

Table 1 lists equations of three simple chaotic jerk systems VE_1-VE_3, depending on the values of a single control parameter c, which corresponds to a_7 in (1), for different families of self-excited and hidden attractors. Table 1 also shows values of parameters (a, b, c), values of an equilibrium $E(x, y, z)$, types of equilibria, and types of attractors. All of the three systems in Table 1 are dissipative.

Table 2 shows eigenvalues, LEs, Lyapunov dimensions D_L (or Kaplan-Yorke dimensions D_{ky}, or attractor dimensions), and initial conditions that are close to the attractor. The Wolf algorithm [46] is employed herein to calculate the LEs based

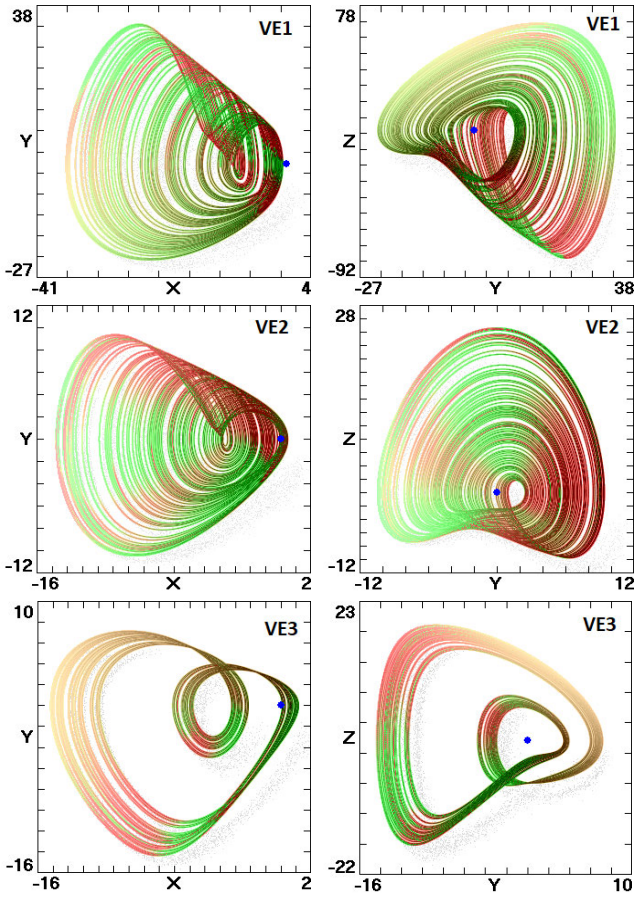

FIGURE 1. Numerical trajectories of three simple chaotic jerk systems with a single all-zero-eigenvalue non-hyperbolic equilibrium in Table 1 projected on (*x, y*) and (*y, z*) planes. The colors in green and red indicate positive and negative values of local LLEs, respectively. The equilibrium points are shown in the blue dots.

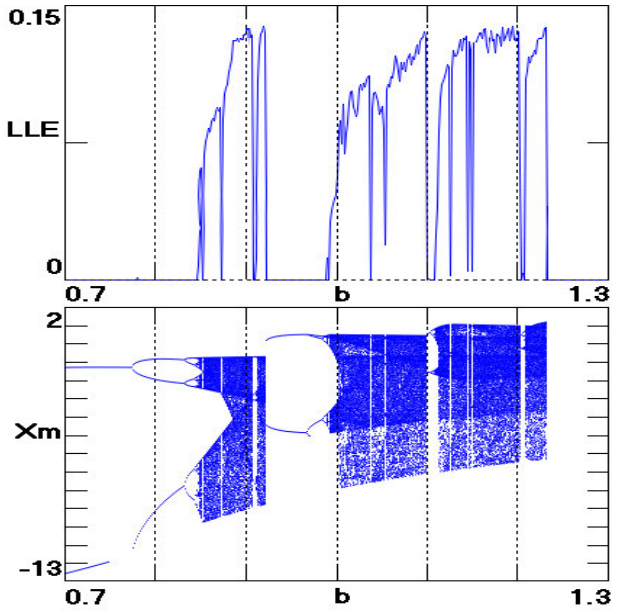

FIGURE 2. The largest Lyapunov exponent and the bifurcation diagram of the system VE_1, with a single all-zero-eigenvalue non-hyperbolic equilibrium, against the parameter *b*.

on the fourth-order Runge-Kutta integrator with a fixed step size (time step = 0.005).

To ensure that chaos is neither transients nor numerical artifacts, the calculations take a sufficiently long time up to time $t = 1 \times 10^8$ [45]. In addition, to avoid uncertainty and determine the approximate number of significant digits of LEs, the calculations of LEs are repeated twice by two slightly different initial conditions (within the basin of attraction), and both calculations are compared. On comparison, the final results of LEs do not quote any digits that are not identical [47].

It can be seen from Table 2 that, as usually found in chaos of 3D autonomous dissipative systems, values of the attractor dimension D_L are only slightly greater than 2.0, whereas the largest D_L is 2.0664 found in the system VE_2 with no equilibria. The parameters of the three systems in Table 1 are in the form of elegant simplicity [45] for which the largest possible values of the positive LE and D_L are reported. Although no efforts are made here, the parameters in Table 1 can be further optimized for the maximum values of the positive LE and D_L, but may not be in the elegant form, by applying the metaheuristic algorithms, e.g., [48]. All the three cases in Table 1 exhibit a period-doubling route to chaos. Based on Cases 1, 2, and 3 in Section II*A*, the three different cases of equilibria are further investigated through examples as follows.

A. CASE 1: A SINGLE NON-HYPERBOLIC EQUILIBRIUM

As mentioned earlier, if $a_7 = c = 0$, the system in (1) will have an all-zero-eigenvalue non-hyperbolic equilibrium at $E(x, y, z) = E_0(0, 0, 0)$, and thus the eigenvalues $\lambda_{1,2,3} = (0, 0, 0)$. This implies that the origin is a center, but it is nonlinearly unstable [49]. Table 1 lists three simple chaotic jerk systems VE_1, VE_2, and VE_3 for $a_7 = c = 0$, and $a_1 = a$, with an all-zero-eigenvalue non-hyperbolic equilibrium.

Fig. 1 depicts the corresponding numerical trajectories of systems VE_1, VE_2, and VE_3 on (x, y) and (y, z) planes. The green and red colors in Fig. 1 indicate positive and negative values, respectively, of the local largest LE (LLE) [33]. The blue dot represents the all-zero-eigenvalue non-hyperbolic equilibrium at the origin. At $a = 1$ and $c = 0$ of the system VE_1 where the LLE is relatively large, Fig. 2 shows the LLE and the bifurcation diagram against the parameter b from 0.7 to 1.3.

For the system VE_1 with a single all-zero-eigenvalue non-hyperbolic equilibrium, Fig. 3 simultaneously visualizes both the Poincare section in black and the basin of attraction in red of the strange attractor, on the same (x, y) plane at $z = 0$. The white background shows the initial conditions that give unbounded orbits. The basin of attraction (red) of the strange attractor occupies a relatively large area compared to the unbounded orbits (white). The attractor is self-excited since

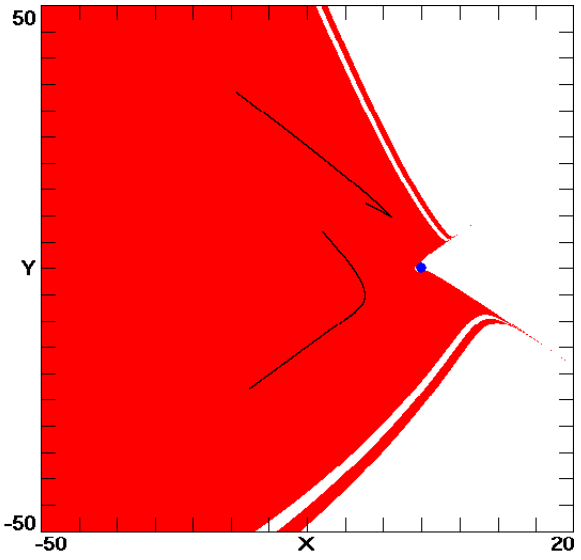

FIGURE 3. The Poincare section in black and the basin of attraction in red of the system VE_1 with a single all-zero-eigenvalue non-hyperbolic equilibrium on the same (x, y) plane at $z = 0$, for $a = 1$, $b = 0.9$ and $c = 0$.

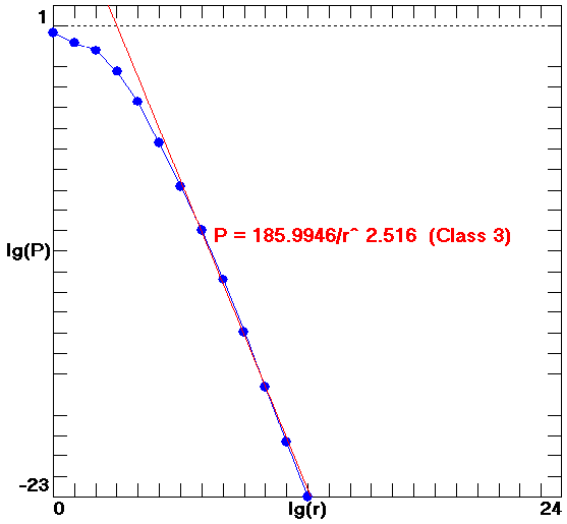

FIGURE 4. The basin of attraction of the system VE_1 with a single all-zero-eigenvalue non-hyperbolic equilibrium is in Class-3, and extends to infinity with a non-integer power-law scaling.

its basin overlaps the equilibrium point indicated by a blue dot [20].

It is known that basins of attraction can be classified into four types [50] depending on their size and extent. To find the attractor basin size, the probability (P) that an initial condition at a distance r from the attractor lies within the basin of attraction can be calculated [50]. According to the classification in [50], the basin of the system VE_1 with a single all-zero-eigenvalue non-hyperbolic equilibrium is in Class-3, in which an arbitrary point at a distance r from the attractor has a probability (P) of being in the basin given approximately by $P = 185.9946/r\text{^}2.516$ in the limit of large r, as shown in Fig. 4, where 'lg' stands for log base 2.

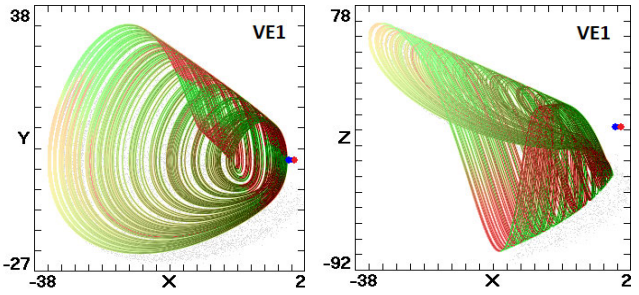

FIGURE 5. Numerical trajectories of the system VE_1 with two symmetrical hyperbolic equilibria for self-excited chaotic attractors on (x, y) and (x, z) planes.

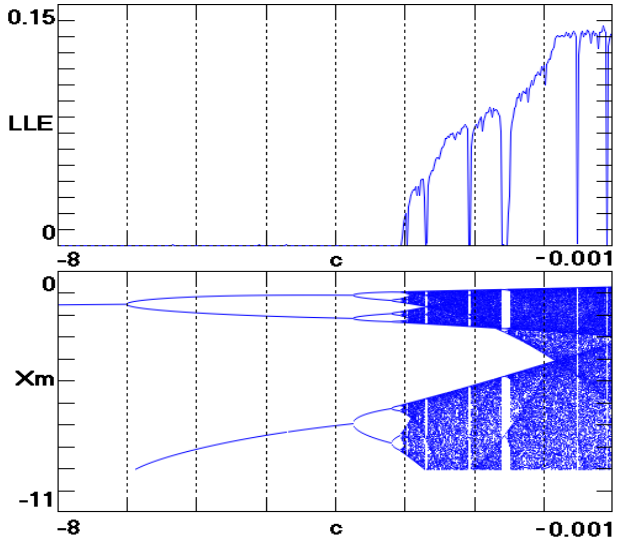

FIGURE 6. The largest Lyapunov exponent and the bifurcation diagram of the system VE_1 with two symmetrical hyperbolic equilibria, against the parameter c.

B. CASE 2: TWO SYMMETRICAL HYPERBOLIC EQUILIBRIA

As mentioned earlier, if $a_7 < 0$, the system in (1) will have two symmetrical hyperbolic equilibria at $E(x, y, z) = E_{1,2} = \left(\pm\sqrt{a_7/a_1}, 0, 0\right)$. Table 1 lists three simple chaotic jerk systems VE_1, VE_2, and VE_3 for $a_7 = (c < 0)$, and $a_1 = a$, with two symmetrical hyperbolic equilibria. For $a = 1$, $b = -a_2 = 0.9$, and $c = -0.2$ of the system VE_1, Table 2 shows that eigenvalues at $E_1 = (0.4472, 0, 0)$ are $\lambda_1^+ = 1.0617$, $\lambda_{2,3}^+ = -0.3967 \pm 0.8277$ and that eigenvalues at $E_2 = (-0.4472, 0, 0)$ are $\lambda_1^- = -1.0617$, $\lambda_{2,3}^- = 0.3967 \pm 0.8277$, where $E_{1,2}$ are of the unstable saddle-focus equilibria. In addition, Table 2 also shows eigenvalues of systems VE_2 and VE_3 evaluated at $E_{1,2} = \left(\pm\sqrt{a_7/a_1}, 0, 0\right)$.

In this case, all the three systems have two symmetrical hyperbolic equilibria $E_{1,2}$ of the unstable saddle-focus type, and therefore all the attractors are self-excited since they are excited from unstable equilibria [20]. As an example, Fig. 5 shows the chaotic attractors of the system VE_1 on (x, y) and (x, z) planes using $a = 1, b = 0.9$, and $c = -0.2$. The red and blue dots represent two symmetrical hyperbolic equilibria at $E_1 = (0.4472, 0, 0)$ and $E_2 = (-0.4472, 0, 0)$, respectively.

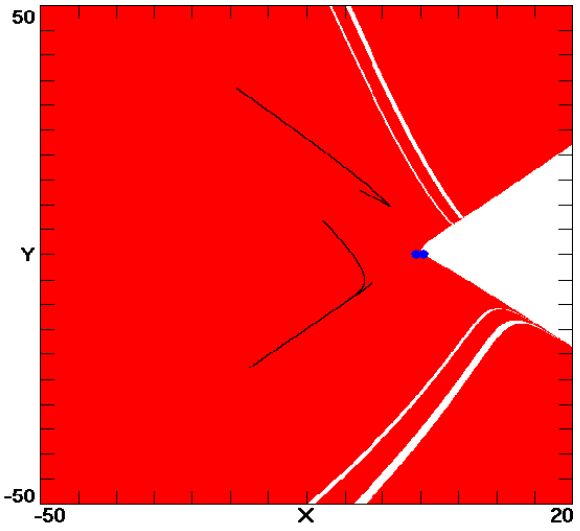

FIGURE 7. The Poincare section in black and the basin of attraction in red of the system VE_1 with two symmetrical hyperbolic equilibria on the same (x, y) plane at $z = 0$ for $a = 1$, $b = 0.9$, and $c = -0.2$.

For $-8 \leq c \leq -0.001$ of the system VE_1 with two symmetrical hyperbolic equilibria, Fig. 6 shows the corresponding numerical results of the LLE and the bifurcation diagram. A period-doubling route to chaos is obvious. In Fig. 6, the highest value of the LLE $= 0.1320$ occurs at $c = -0.2$. Fig. 7 shows both the Poincare section in black and the basin of attraction in red of the system VE_1 with two symmetrical hyperbolic equilibria, on the same (x, y) plane at $z = 0$.

In Fig. 7, initial conditions in red lead to the chaotic attractor, and initial conditions in white lead to unbounded solutions. The attractor is self-excited since its basin overlaps both equilibrium points $E_{1,2}$ indicated by two blue dots in Fig. 7. In addition, the (red) basin of the system VE_1 with two symmetrical hyperbolic equilibria in Fig. 7 occupies a relatively large area compared to the (red) basin of the system VE_1 with a single all-zero-eigenvalue non-hyperbolic equilibrium in Fig. 3.

C. CASE 3: NO EQUILIBRIA

As mentioned earlier, if $a_7 > 0$, the system in (1) will have no equilibria, and therefore attractors are readily hidden [20]. Table 1 lists three simple chaotic jerk systems VE_1, VE_2, and VE_3 for $a_7 = (c > 0)$, and $a_1 = a$, with no equilibria, but they can show chaotic behavior. For $a = 1$, $b = -a_2 = 0.9$, and $c = 0.24$ of the system VE_1 with no equilibria, Fig. 8 shows the corresponding numerical trajectories projected onto (x, y) and (x, z) planes.

For the system VE_1, although the shape of the chaotic attractors in Fig. 8 with no equilibria (Case 3) resembles the chaotic attractors in Fig. 1 with a single all-zero-eigenvalue non-hyperbolic equilibrium (Case 1), or in Fig. 5 with two symmetrical hyperbolic equilibria (Case 2), the main

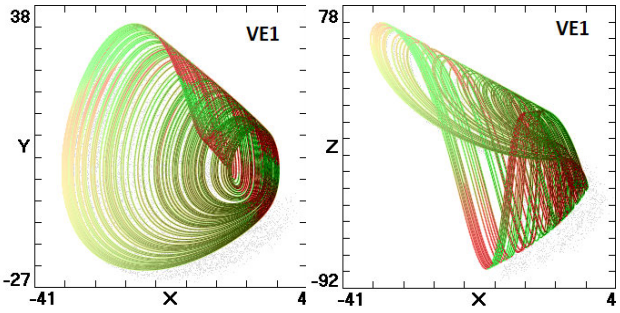

FIGURE 8. Numerical trajectories of the system VE_1 with no equilibria for hidden chaotic attractors on (x, y) and (x, z) planes.

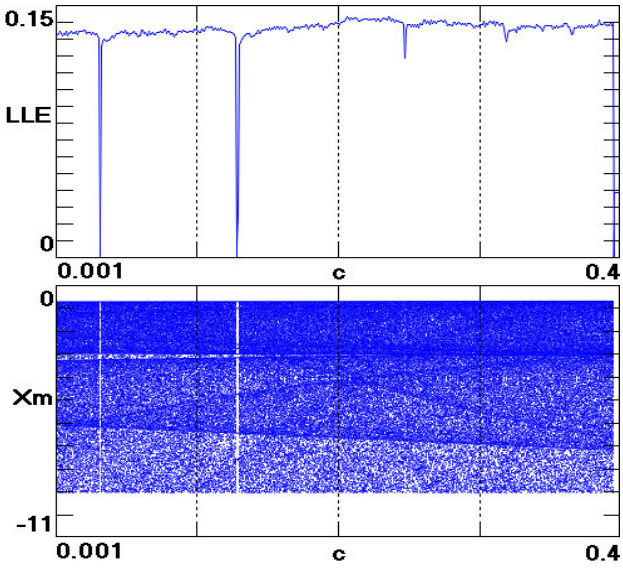

FIGURE 9. The largest Lyapunov exponent and the bifurcation diagram of the system VE_1 with no equilibria, against the parameter c.

difference is that the chaotic attractors in Fig. 8 with no equilibria (Case 3) are hidden.

For $a = 1$ and $b = 0.9$ of the system VE_1 with no equilibria, Fig. 9 numerically shows the LLE and the bifurcation diagram versus the parameter c from 0.001 to 0.4. In Fig. 9, most values of the LLE are relatively maintained near 0.1410 with only two narrow periodic windows.

D. REGIONS OF DYNAMICAL BEHAVIOR FOR SELF-EXCITED AND HIDDEN ATTRACTORS

As shown in Table 1, the parameter c is the controller of dynamical behavior of the three chaotic jerk systems VE_1, VE_2, and VE_3, as different values of c change types of equilibria and attractors. As an example, such changes are particularly demonstrated through the system VE_1. In an attempt to find relationships between the control parameter c and the bifurcation parameter b of the system VE_1, Fig. 10 plots regions of dynamical behavior, which are based on the spectrum of LEs (L_1, L_2, L_3) and are essentially

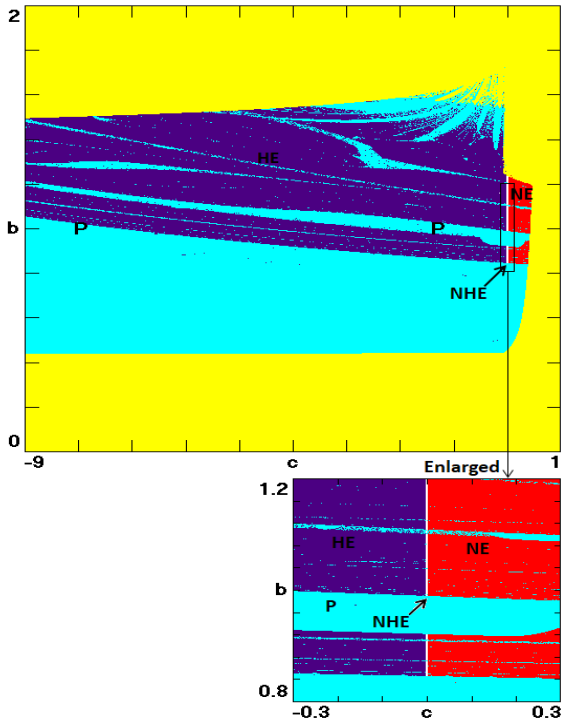

FIGURE 10. For the system VE_1, regions of dynamical behavior consist of five colored pixels for six different attractors on a [c, b] plane, with different families of self-excited and hidden attractors. Pixels in white, purple, and red for $c = 0$, $c < 0$, and $c > 0$ represent chaotic attractors with a single NHE, two symmetrical HE, and NE, respectively. Pixels in cyan for $c = 0$, $c < 0$, and $c > 0$ represent periodic attractors with a single NHE, two symmetrical HE, and NE, respectively. Pixels in yellow refer to unbounded solutions. An inset in the vicinity of the white pixels with the NHE is enlarged.

bifurcation diagrams on a two-parameter (c, b) plane, for $-9 \leq c \leq 1$ and $0 \leq b \leq 2$.

In Fig. 10, initial conditions are fixed at (0.1, 0.6, −0.8) for the whole parameter space of 512 × 512 pixels, and the regions of dynamical behavior − with different families of self-excited and hidden attractors − consist of five colored pixels for six different attractors as follows:

1) Pixels in white represent self-excited chaotic attractors with a single all-zero-eigenvalue non-hyperbolic equilibrium (NHE) for $c = 0$.
2) Pixels in purple represent self-excited chaotic attractors with two symmetrical hyperbolic equilibria (HE) for $c < 0$.
3) Pixels in red represent hidden chaotic attractors with no equilibria (NE) for $c > 0$.
4) Pixels in cyan represent self-excited periodic attractors (P) with a single all-zero-eigenvalue non-hyperbolic equilibrium (NHE) for $c = 0$.
5) Pixels in cyan represent self-excited periodic attractors (P) with two symmetrical hyperbolic equilibrium (HE) for $c < 0$.
6) Pixels in cyan represent hidden periodic attractors (P) with no equilibria (NE) for $c > 0$.
7) Pixels in yellow lead to unbounded solutions.

Fig. 10 also includes an enlarged inset in the vicinity of the white pixels of chaotic attractors with a single all-zero-eigenvalue NHE ($c = 0$) of the system VE_1. The inset clearly shows that the white pixels occupy a tiny thin line mainly surrounded by the purple pixels (on the left), the red pixels (on the right), and the cyan pixels. It can be seen from Fig. 10 that the purple pixels of chaotic attractors with two symmetrical HE occupy a relatively large two-parameter space compared with either a smaller area of the red pixels of chaotic attractors with NE, or a much smaller thin line of the white pixels of chaotic attractors with a single all-zero-eigenvalue NHE.

IV. FREE CONTROL OF AMPLITUDE, FREQUENCY, AND POLARITY

A. FREE CONTROL OF CHAOTIC SIGNALS

A dynamical system has amplitude parameters and bifurcation parameters [33], which influence the size of the attractor and its topology, respectively. When $c = 0$, systems VE_1-VE_3 in Table 1 with a single all-zero-eigenvalue non-hyperbolic equilibrium, have only two linear terms. The coefficient of the two linear terms y and z controls both the amplitude and frequency [13] of the signals generated by the systems since these are the only terms whose dimensions are different from the remaining quadratic terms. Also, the systems in Table 1 with a single all-zero-eigenvalue non-hyperbolic equilibrium provide polarity control [31], by the introduction of a new constant in the variable x.

As an illustration, consider a simultaneous amplitude, frequency, and polarity control of the system VE_1 with a single all-zero-eigenvalue non-hyperbolic equilibrium by the transformation $x \to (x + n)/m$, $y \to y/m$, $z \to z/m$ and $t \to mt$. The system VE_1 becomes

$$\begin{cases} \dot{x} = my \\ \dot{y} = mz \\ \dot{z} = a\,(x+n)^2 - by^2 + 0.6\,(x+n)\,z + 0.4yz \end{cases} \tag{2}$$

Therefore, the newly introduced coefficient m of the linear terms in (2) provides both amplitude and frequency control of chaotic signals according to m, while the constant n provides polarity control allowing a transformation between a bipolar signal and a unipolar signal of the variable x. The polarity controller n should be adjusted to maintain a unipolar or bipolar signal according to the controller m. For simplicity in the next subsection, the parameter values of the system (2) are fixed at $a = 1$, $b = 0.9$, and initial conditions at (0.1, 0.6, −0.8), unless stated otherwise.

B. SIMULTANEOUS AMPLITUDE, FREQUENCY, AND POLARITY CONTROL OF CHAOTIC SIGNALS

Fig. 11 illustrates three examples of chaotic signals from the system (2) for different values of the amplitude-frequency controller m and the polarity controller n. A high amplitude-frequency bipolar signal x in green at the center for $m = 2$ and $n = -35$, a medium amplitude-frequency negative unipolar signal x in red at the lower half for $m = 1$ and $n = 0$, and a low

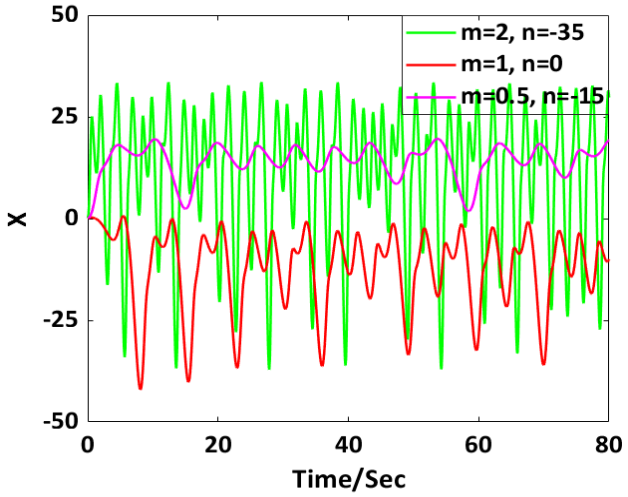

FIGURE 11. Three chaotic signals $x(t)$ from the system (2) for different values of the amplitude-frequency controller m and the polarity controller n.

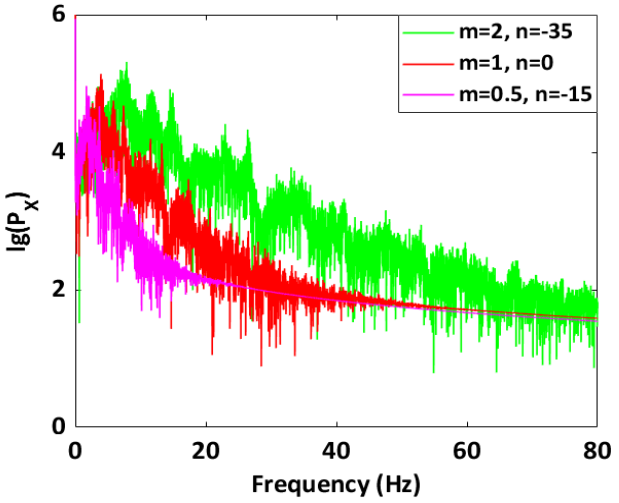

FIGURE 13. The frequency spectrum of the signal x for different values of the amplitude-frequency controller m and the polarity controller n.

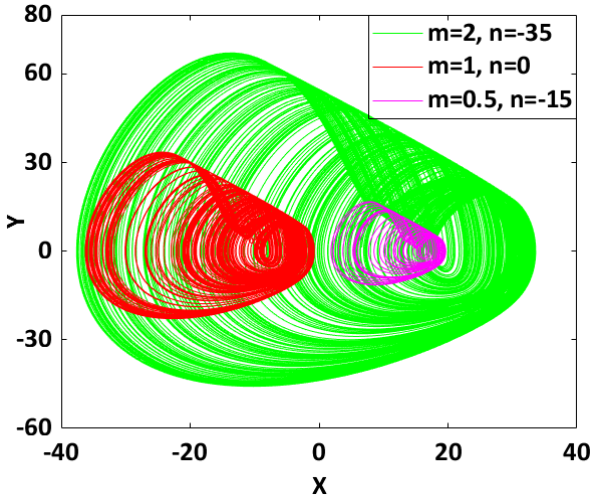

FIGURE 12. A high amplitude-frequency bipolar signal in green for $m = 2$, $n = -35$, a medium amplitude-frequency negative unipolar signal in red for $m = 1$, $n = 0$, and a low amplitude-frequency positive unipolar signal in pink for $m = 0.5$, $n = -15$.

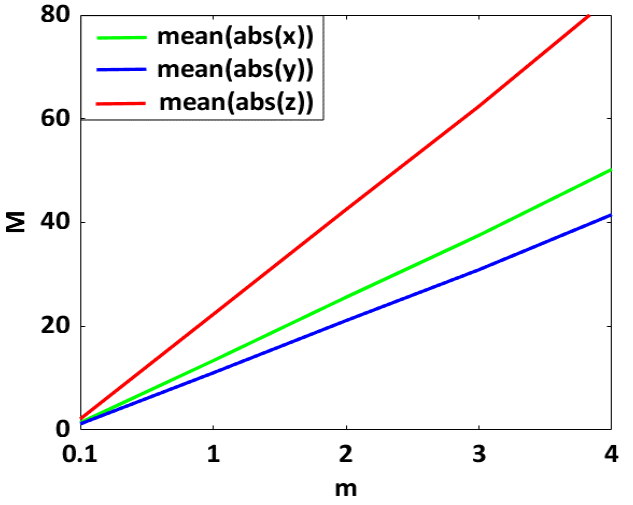

FIGURE 14. Linearly rescaled mean values of $|x|$, $|y|$ and $|z|$ versus the amplitude-frequency controller m varies from 0.1 to 4, for $n = 0$.

amplitude-frequency positive unipolar signal x in pink at the upper half for $m = 0.5$ and $n = -15$. A more clear illustration is shown in Fig. 12, where phase trajectories on an (x, y) plane are controlled and shifted simultaneously by the controller m and n. The corresponding different frequency spectra of the signal x are shown in Fig. 13.

To prove the free control of amplitude and frequency scaling theoretically, Fig. 14 shows that in the system (2) when the amplitude-frequency controller m, namely, the coefficient of the linear terms in the first and second dimension, varies from 0.1 to 4, an average of absolute value signals $|x|$, $|y|$, and $|z|$ is rescaled in proportion to the controller m. Fig. 15 shows that the LEs are also rescaled with the controller m since it also controls the frequency of the signals [33]. For the sake of clarity, only a small portion of the most negative LE (LE3) has been shown in Fig. 15.

At $m = 1$, Fig. 16 shows mean values of x, y, and z versus the polarity controller n. It can be seen from Fig. 16 that n only changes the mean value of x, but does not influence the mean values of y and z, indicating that n is the polarity controller of the variable x. In particular, the spectrum of LEs (LE_1, LE_2, LE_3) remains relatively unchanged for $-35 \leq n \leq 0$, as shown in Fig. 17. As a result, the change of n introduces no effects on the dynamics but provides a controllable level shift for practical applications where a chaotic signal of particular polarity is required, e.g., [36].

V. CIRCUIT REALIZATION

The hardware implementation of mathematical chaotic models is important for practical applications, e.g., chaos-based

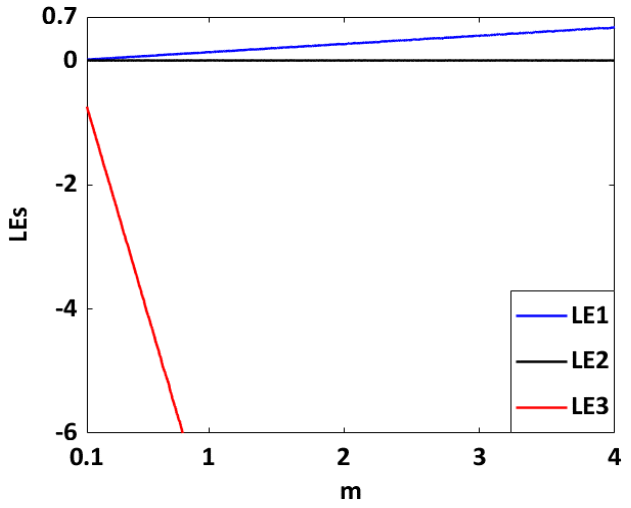

FIGURE 15. Linearly rescaled Lyapunov exponents versus the amplitude-frequency controller m varies from 0.1 to 4, for $n = 0$.

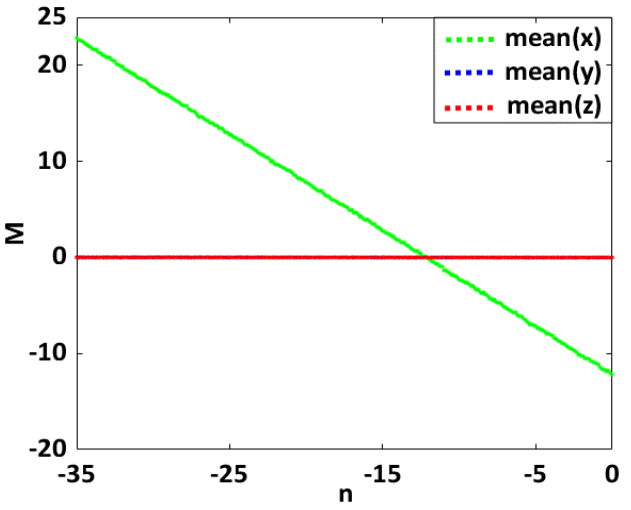

FIGURE 16. Mean values of x, y, and z versus the polarity controller n from −35 to 0, for $m = 1$.

secure communications [34], [39]. Analog and digital approaches have been applied to practically realize chaotic systems by using, e.g., integrated circuits (ICs) [51], [52], Field-Programmable Gate Arrays (FPGAs) [53], [54], and commercially available operational amplifiers (op-amps) [33], [40]. Also, the synchronization of chaotic systems and applications to chaos-based secure communications have been demonstrated using ICs [55] and FPGAs [56].

The ICs design of chaotic systems requires an optimization to avoid the variations problems from IC fabrication technologies [51], where a variation in a process, voltage, or temperature (PVT) may degrade or even eliminate the chaotic behavior. For FPGA-based implementation, an appropriate numerical method should be selected to discretize the mathematical model of a chaotic system [54]. In addition, when designing chaotic circuits with op-amps, frequency limitations should be considered carefully [57].

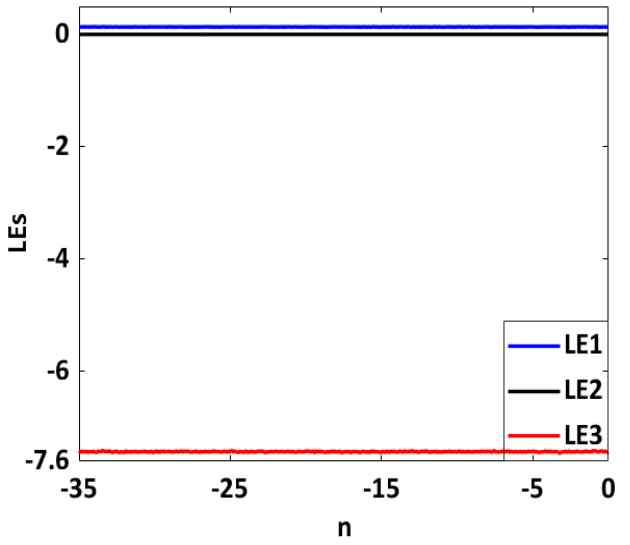

FIGURE 17. The relatively unchanged spectrum of LEs (*LE1*, *LE2*, *LE3*) versus the polarity controller n from −35 to 0, for $m = 1$.

In this section, an analog electronic circuit is physically constructed to realize (2). According to the numerical trajectories of the system VE_1, with a single all-zero-eigenvalue non-hyperbolic equilibrium, in Fig. 1, the ranges of the variables x, y, and z (in volts) do not satisfy the requirement of not saturating the op-amps and analog multipliers. To prevent the op-amps and analog multipliers from saturating, the transformation $x = 10X$, $y = 10Y$, and $z = 10Z$ is used with the minification factor of 10. The scaled equations of (2) are given by

$$\begin{cases} \dot{X} = mY \\ \dot{Y} = mZ \\ \dot{Z} = 10a\,(X + n/10)^2 - 10bY^2 + 6\,(X + n/10)\,Z + 4YZ \end{cases} \tag{3}$$

Fig. 18 shows an electronic circuit that emulates (3). The circuit consists of three op-amps U_1 to U_3 for the three integration channels, three op-amps U_4 to U_6 for the inverting amplifiers, one op-amp U_7 for the summing amplifier, and four analog multipliers U_8 to U_{11} (using AD633 with an implied voltage factor of 1) for the four terms of quadratic nonlinearity. All the op-amps are TL082 ICs powered by ±15V. A set of three coupled first-order ODEs of the circuit is

$$\begin{cases} \dot{X} = \dfrac{1}{RC_1}\left(\dfrac{R}{R_1}Y\right) \\ \dot{Y} = \dfrac{1}{RC_2}\left(\dfrac{R}{R_9}Z\right) \\ \dot{Z} = \dfrac{1}{RC_3}\left(\dfrac{R}{R_{12}}(X - V_d)^2 - \dfrac{R}{R_{13}}Y^2 \right. \\ \qquad \left. + \dfrac{R}{R_{14}}(X - V_d)\,Z + \dfrac{R}{R_{15}}YZ\right) \end{cases} \tag{4}$$

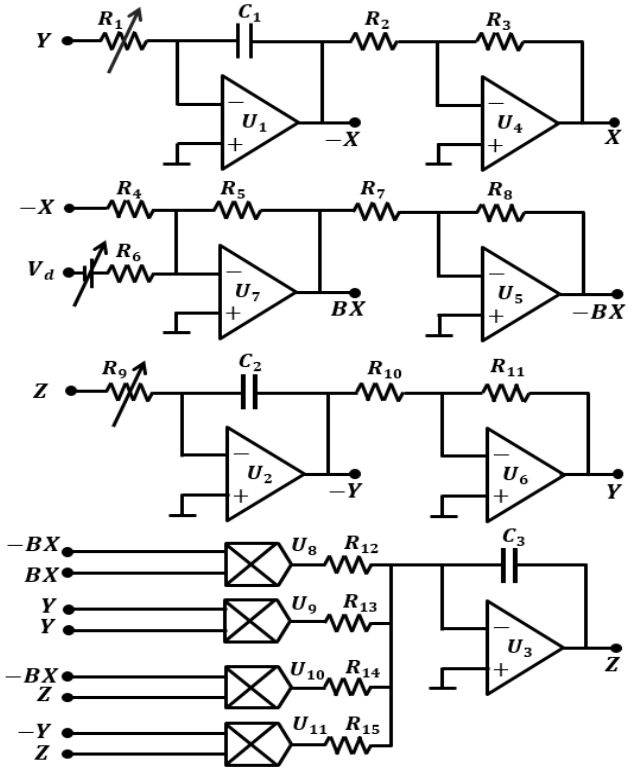

FIGURE 18. Circuit realization of the scaled system (3) with a single all-zero-eigenvalue non-hyperbolic equilibrium for free control of amplitude, frequency, and polarity.

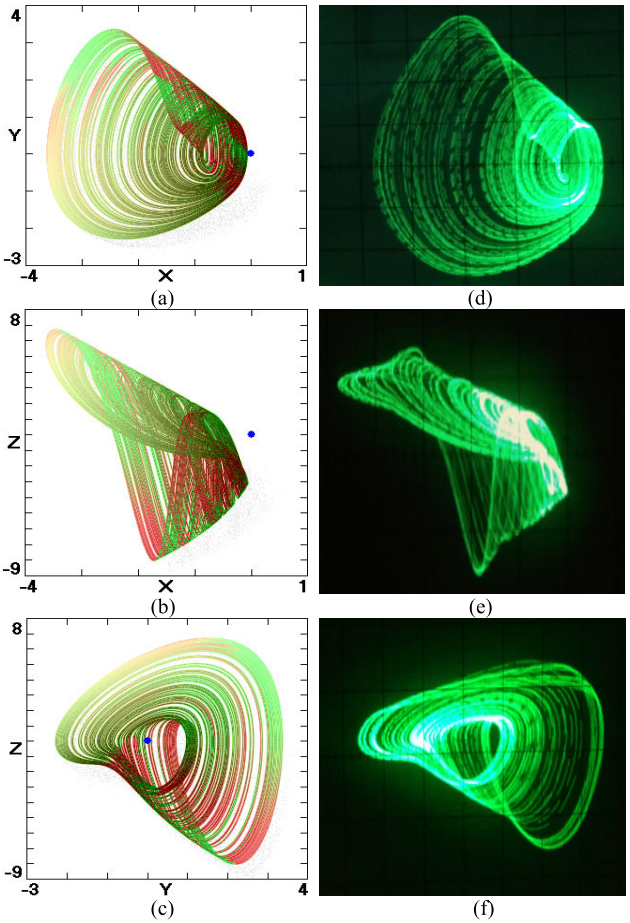

FIGURE 19. Trajectories of the scaled system (3) on (X, Y), (X, Z), and (Y, Z) planes respectively for (a)−(c) numerical results, and for (d)−(f) oscilloscope traces (X: 1V/div, Y: 1V/div, and Z: 5V/div) using $a = 1$, $b = 0.9$, $m = 1$, and $n = 0$.

Equation (4) corresponds to (3), where the phase space variables X, Y, and Z represent the output voltages of the three integration channels U_1 to U_3 and two inverting amplifiers U_4 and U_6, whereas BX is the output voltage of the summing amplifier U_7 which provides the polarity control $(X - V_d)$ of the variable X according to the adjustable DC voltage source V_d. By normalizing the differential equations of the system (4) for $\tau = t/RC$, where $C = C_1 = C_2 = C_3$, this system is equivalent to (3), with $R/R_1 = R/R_9 = m$, $R/R_{12} = 10a$, $V_d = n/10$, $R/R_{13} = 10b$, $R/R_{14} = 6$, and $R/R_{15} = 4$.

Unlike other chaotic circuits, two potentiometers R_1 and R_9 in Fig. 18 are used to control the amplitude and frequency of the chaotic signals. By these knobs, the signals X, Y, and Z for any desired amplitude and frequency can be adjusted. With a decrease or increase in R_1 and R_9, the amplitude and frequency of the variables (X, Y, Z) increase or decrease accordingly. The polarity control of the signal X can be achieved by the adjustable DC voltage source V_d.

For $a = 1$, $b = 0.9$, $m = 1$, and $n = 0$, numerical trajectories and oscilloscope traces of the scaled system (3) are illustrated in Figs. 19(a)−19(c) and Figs. 19(d)−19(f), respectively, on (X, Y), (X, Z), and (Y, Z) planes, respectively, using $V_d = 0$, $C = C_1 = C_2 = C_3 = 10$ nF, $R = R_1 = R_2 = R_3 = R_4 = R_5 = R_6 = R_7 = R_8 = R_9 = R_{10} = R_{11} = 100$ kΩ, $R_{12} = 10$ kΩ, $R_{13} = 11.11$ kΩ, $R_{14} = 16.67$ kΩ and $R_{15} = 25$ kΩ. The capacitor values are selected to obtain a stable phase portrait which only affects the time scale of the oscillation [35]. The numerical and experimental results are consistent on the (X, Y) plane. However, the experimental results on the (X, Z) and (Y, Z) planes are not totally similar to the numerical results because of non-ideal behaviors of the analog multipliers (U_8 to U_{11}) [58], which are used to implement the four quadratic terms of nonlinearity in the third equation of the system (3).

As mentioned earlier, the amplitude-frequency controller m is adjustable by two potentiometers R_1 and R_9, while the polarity controller n is adjustable by the DC voltage source V_d. The oscilloscope traces of low amplitude and frequency for $m = 0.5$ and $n = -15$ using $R_1 = R_9 = 200$ kΩ and $V_d = 1.5V$, respectively, are shown in Fig. 20 (a). Similarly, the oscilloscope traces of high amplitude and frequency for $m = 2$ and $n = -35$ using $R_1 = R_9 = 50$ kΩ and $V_d = 3.5V$, respectively, are shown in Fig. 20 (b). The corresponding time-series of the signals X for different values of the amplitude-frequency controller m and the polarity controller n are shown in Fig. 21(a)−21(c).

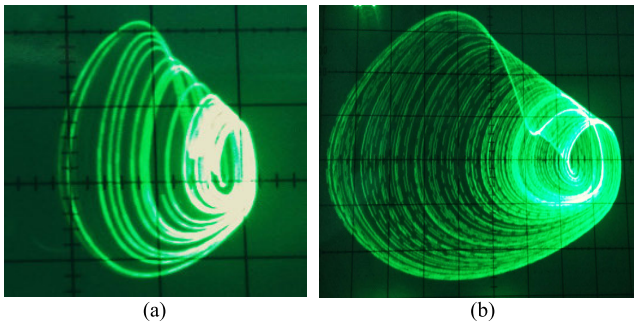

FIGURE 20. Oscilloscope traces of the scaled system (3) on (X, Y) plane (X: 1V/div, Y: 1V/div) for different values of the amplitude-frequency controller m and the polarity controller n (a) $m = 0.5$, $n = -15$ (b) $m = 2$, $n = -35$.

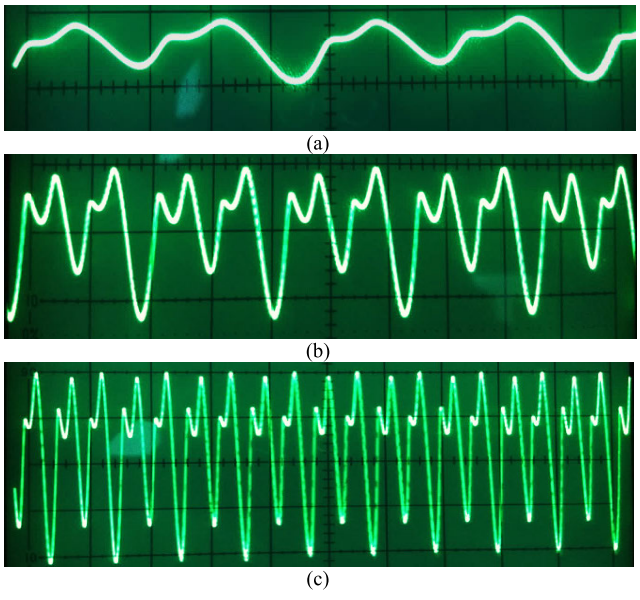

FIGURE 21. Three chaotic signals $X(t)$ (X: 2V/div) from the scaled system (3) for different values of the amplitude-frequency controller m and the polarity controller n (a) $m = 0.5$, $n = -15$ (b) $m = 1$, $n = 0$ (c) $m = 2$, $n = -35$.

VI. CONCLUSIONS

In this paper, using an exhaustive computer search, three simple chaotic jerk systems, of the form of equation (1), are presented for different families of self-excited and hidden attractors. Depending on the values of the single control parameter, the attractors of these systems can change itself between self-excited and hidden attractors. In the family of self-excited attractors, the systems can have a single all-zero-eigenvalue non-hyperbolic equilibrium or two symmetrical hyperbolic equilibria. Besides, for a particular value of the control parameter, the attractors with no equilibria are hidden.

For a single all-zero-eigenvalue non-hyperbolic equilibrium, these systems have only two linear terms, whose coefficient provides a good control knob for amplitude and frequency adjustment. In addition, the introduction of a new constant in the variables x in the third dimension provides a polarity control allowing a transformation between a bipolar signal and a unipolar signal. The amplitude-frequency controller linearly rescales mean values of the signals (x, y, z) and the LEs (as a result of the time rescaling) [33] without encountering undesirable bifurcations [17], [35]. The polarity controller only rescales the mean value of the signal x but does not influence the LEs, leading to the same dynamics of the systems [31].

When implemented as an electronic circuit, these controllers only require two independent potentiometers or variable resistors and an adjustable DC voltage source, which eliminates the need for a more complicated circuit for chaos applications [31], [35]. Finally, as an example, an experimental circuit realization of the system VE_1 with a single all-zero-eigenvalue non-hyperbolic equilibrium demonstrates that these systems can provide chaotic signals with any desired amplitude, frequency, and polarity; therefore, they should have broad applications in engineering, e.g., chaos-based secure communications.

ACKNOWLEDGMENT

The programs used for the exhaustive computer search, analysis, and many of the figures were written by Prof. J. C. Sprott and are used with his permission.

REFERENCES

[1] B. Srisuchinwong and B. Munmuangsaen, "Four current-tunable chaotic oscillators in set of two diode-reversible pairs," *Electron. Lett.*, vol. 48, no. 17, pp. 1051–1053, Aug. 2012.
[2] B. Srisuchinwong and R. Treetanakorn, "Current-tunable chaotic jerk circuit based on only one unity-gain amplifier," *Electron. Lett.*, vol. 50, no. 24, pp. 1815–1817, Nov. 2014.
[3] B. Munmuangsaen and B. Srisuchinwong, "A minimum five-component five-term single-nonlinearity chaotic jerk circuit based on a twin-jerk single-op-amp technique," *Int. J. Circuit Theory Appl.*, vol. 46, no. 3, pp. 656–670, Mar. 2018.
[4] J. Kengne, Z. T. Njitacke, and H. B. Fotsin, "Dynamical analysis of a simple autonomous jerk system with multiple attractors," *Nonlinear Dyn.*, vol. 83, nos. 1–2, pp. 751–765, Jan. 2016.
[5] J. H. Bickford, *Mechanisms for Intermittent Motion*. New York, NY, USA: Industrial Press, 1972.
[6] A. Carolina Sparavigna, "Jerk and hyperjerk in a rotating frame of reference," *Int. J. Sci.*, vol. 1, no. 3, pp. 29–33, 2015.
[7] J. C. Sprott and S. J. Linz, "Algebraically simple chaotic flows," *Int. J. Chaos Theory Appl.*, vol. 5, no. 2, pp. 1–20, Jan. 2000.
[8] J. C. Sprott, "Some simple chaotic jerk functions," *Amer. J. Phys.*, vol. 65, no. 6, pp. 537–543, Jun. 1997.
[9] J. C. Sprott, "Strange attractors with various equilibrium types," *Eur. Phys. J. Special Topics*, vol. 224, no. 8, pp. 1409–1419, Jul. 2015.
[10] L. P. Shilnikov, A. L. Shilnikov, D. V Turaev, and L. O. Chua, *Methods of Qualitative Theory in Nonlinear Dynamics*, vol. 5. Singapore: World Scientific, 2001.
[11] B. Chen, T. Zhou, and G. Chen, "An extended šil'nikov homoclinic theorem and its applications," *Int. J. Bifurcation Chaos*, vol. 19, no. 5, pp. 1679–1693, 2009.
[12] C.-L. Li, H.-M. Li, W. Li, Y.-N. Tong, J. Zhang, D.-Q. Wei, and F.-D. Li, "Dynamics, implementation and stability of a chaotic system with coexistence of hyperbolic and non-hyperbolic equilibria," *AEU-Int. J. Electron. Commun.*, vol. 84, pp. 199–205, Feb. 2018.
[13] Z. Wei, J. C. Sprott, and H. Chen, "Elementary quadratic chaotic flows with a single non-hyperbolic equilibrium," *Phys. Lett. A*, vol. 379, no. 37, pp. 2184–2187, Oct. 2015.
[14] Z. Wei, W. Zhang, and M. Yao, "On the periodic orbit bifurcating from one single non-hyperbolic equilibrium in a chaotic jerk system," *Nonlinear Dyn.*, vol. 82, no. 3, pp. 1251–1258, Jul. 2015.

[15] K. Rajagopal, V.-T. Pham, F. R. Tahir, A. Akgul, H. R. Abdolmohammadi, and S. Jafari, "A chaotic jerk system with non-hyperbolic equilibrium: Dynamics, effect of time delay and circuit realisation," *Pramana*, vol. 90, no. 4, pp. 1–8, Mar. 2018.

[16] T. Zhou and G. Chen, "Classification of chaos in 3-D autonomous quadratic systems-I: Basic framework and methods," *Int. J. Bifurcation Chaos*, vol. 16, no. 9, pp. 2459–2479, 2006.

[17] C. Li and J. C. Sprott, "Chaotic flows with a single nonquadratic term," *Phys. Lett. A*, vol. 378, no. 3, pp. 178–183, Jan. 2014.

[18] N. V. Kuznetsov, G. A. Leonov, and V. I. Vagaitsev, "Analytical-numerical method for attractor localization of generalized Chua's system," *IFAC Proc. Volumes*, vol. 43, no. 11, pp. 29–33, Aug. 2010.

[19] G. A. Leonov, N. V. Kuznetsov, O. A. Kuznetsova, S. M. Seledzhi, and V. I. Vagaitsev, "Hidden oscillations in dynamical systems," *Trans. Syst. Control*, vol. 6, no. 2, pp. 54–67, Feb. 2011.

[20] G. A. Leonov, N. V. Kuznetsov, and T. N. Mokaev, "Homoclinic orbits, and self-excited and hidden attractors in a lorenz-like system describing convective fluid motion," *Eur. Phys. J. Special Topics*, vol. 224, no. 8, pp. 1421–1458, Jul. 2015.

[21] S. Jafari, J. C. Sprott, and F. Nazarimehr, "Recent new examples of hidden attractors," *Eur. Phys. J. Special Topics*, vol. 224, no. 8, pp. 1469–1476, Jul. 2015.

[22] B. Munmuangsaen and B. Srisuchinwong, "A hidden chaotic attractor in the classical lorenz system," *Chaos, Solitons Fractals*, vol. 107, pp. 61–66, Feb. 2018.

[23] B. R. Andrievsky, N. V. Kuznetsov, G. A. Leonov, and A. Y. Pogromsky, "Hidden oscillations in aircraft flight control system with input saturation," *IFAC Proc. Volumes*, vol. 46, no. 12, pp. 75–79, Jan. 2013.

[24] G. A. Leonov, N. V. Kuznetsov, M. A. Kiseleva, E. P. Solovyeva, and A. M. Zaretskiy, "Hidden oscillations in mathematical model of drilling system actuated by induction motor with a wound rotor," *Nonlinear Dyn.*, vol. 77, nos. 1–2, pp. 277–288, Mar. 2014.

[25] I. Ahmad, B. Srisuchinwong, and W. San-Um, "On the first hyperchaotic hyperjerk system with no equilibria: A simple circuit for hidden attractors," *IEEE Access*, vol. 6, pp. 35449–35456, 2018.

[26] S. Jafari, J. C. Sprott, V.-T. Pham, C. Volos, and C. Li, "Simple chaotic 3D flows with surfaces of equilibria," *Nonlinear Dyn.*, vol. 86, no. 2, pp. 1349–1358, Jul. 2016.

[27] K. Barati, S. Jafari, J. C. Sprott, and V.-T. Pham, "Simple chaotic flows with a curve of equilibria," *Int. J. Bifurcation Chaos*, vol. 26, no. 12, Nov. 2016, Art. no. 1630034.

[28] B. Srisuchinwong, B. Munmuangsaen, I. Ahmad, and K. Suibkitwanchai, "On a simple single-transistor-based chaotic snap circuit: A maximized attractor dimension at minimized damping and a stable equilibrium," *IEEE Access*, vol. 7, pp. 116643–116660, 2019.

[29] W. Hu, A. Akgul, C. Li, T. Zheng, and P. Li, "A switchable chaotic oscillator with two amplitude-frequency controllers," *J. Circuits, Syst. Comput.*, vol. 26, no. 10, Feb. 2017, Art. no. 1750158.

[30] C. Li, J. C. Sprott, and H. Xing, "Constructing chaotic systems with conditional symmetry," *Nonlinear Dyn.*, vol. 87, no. 2, pp. 1351–1358, Jan. 2017.

[31] C. Li and J. C. Sprott, "Variable-boostable chaotic flows," *Optik*, vol. 127, no. 22, pp. 10389–10398, Nov. 2016.

[32] C. Li and J. C. Sprott, "Amplitude control approach for chaotic signals," *Nonlinear Dyn.*, vol. 73, no. 3, pp. 1335–1341, Mar. 2013.

[33] C. Li, J. C. Sprott, Z. Yuan, and H. Li, "Constructing chaotic systems with total amplitude control," *Int. J. Bifurcation Chaos*, vol. 25, no. 10, Sep. 2015, Art. no. 1530025.

[34] B. Srisuchinwong and B. Munmuangsaen, "Secure communication systems based upon two-fold masking of different chaotic attractors, including modified chaotic attractors, using static-dynamic secret keys," WO Patent 105 972, Sep. 1, 2011. [Online]. Available: https://patentscope.wipo.int/search/en/detail.jsf?docId=WO2011105972&tab=PCTBIBLIO

[35] C. Li, J. C. Sprott, A. Akgul, H. H. C. Iu, and Y. Zhao, "A new chaotic oscillator with free control," *Chaos, Interdiscipl. J. Nonlinear Sci.*, vol. 27, no. 8, Aug. 2017, Art. no. 083101.

[36] I. Obeid, J. C. Morizio, K. A. Moxon, M. A. L. Nicolelis, and P. D. Wolf, "Two multichannel integrated circuits for neural recording and signal processing," *IEEE Trans. Biomed. Eng.*, vol. 50, no. 2, pp. 255–258, Feb. 2003.

[37] C. Li, J. Wang, and W. Hu, "Absolute term introduced to rebuild the chaotic attractor with constant Lyapunov exponent spectrum," *Nonlinear Dyn.*, vol. 68, no. 4, pp. 575–587, Jun. 2012.

[38] S. Jafari, J. C. Sprott, and S. M. R. Hashemi Golpayegani, "Elementary quadratic chaotic flows with no equilibria," *Phys. Lett. A*, vol. 377, no. 9, pp. 699–702, Mar. 2013.

[39] M. A. Jafari, E. Mliki, A. Akgul, V.-T. Pham, S. T. Kingni, X. Wang, and S. Jafari, "Chameleon: The most hidden chaotic flow," *Nonlinear Dyn.*, vol. 88, no. 3, pp. 2303–2317, May 2017.

[40] K. Rajagopal, A. Akgul, S. Jafari, A. Karthikeyan, and I. Koyuncu, "Chaotic chameleon: Dynamic analyses, circuit implementation, FPGA design and fractional-order form with basic analyses," *Chaos, Solitons Fractals*, vol. 103, pp. 476–487, Oct. 2017.

[41] F. Nazarimehr, K. Rajagopal, J. Kengne, S. Jafari, and V.-T. Pham, "A new four-dimensional system containing chaotic or hyper-chaotic attractors with no equilibrium, a line of equilibria and unstable equilibria," *Chaos, Solitons Fractals*, vol. 111, pp. 108–118, Jun. 2018.

[42] J. Munoz-Pacheco, E. Zambrano-Serrano, C. Volos, S. Jafari, J. Kengne, and K. Rajagopal, "A new fractional-order chaotic system with different families of hidden and self-excited attractors," *Entropy*, vol. 20, no. 8, p. 564, Jul. 2018.

[43] K. Rajagopal, S. Jafari, A. Akgul, and A. Karthikeyan, "Modified jerk system with self-exciting and hidden flows and the effect of time delays on existence of multi-stability," *Nonlinear Dyn.*, vol. 93, no. 3, pp. 1087–1108, Apr. 2018.

[44] S. T. Kingni, G. F. Kuiate, V. K. Tamba, V.-T. Pham, and D. V. Hoang, "Self-excited and hidden attractors in an autonomous josephson jerk oscillator: Analysis and its application to text encryption," *J. Comput. Nonlinear Dyn.*, vol. 14, no. 7, May 2019, Art. no. 071004.

[45] J. C. Sprott, *Elegant Chaos: Algebraically Simple Chaotic Flows*. Singapore: World Scientific, 2010.

[46] A. Wolf, J. B. Swift, H. L. Swinney, and J. A. Vastano, "Determining Lyapunov exponents from a time series," *Phys. D, Nonlinear Phenomena*, vol. 16, no. 3, pp. 285–317, Jul. 1985.

[47] J. C. Sprott, "A proposed standard for the publication of new chaotic systems," *Int. J. Bifurcation Chaos*, vol. 21, no. 9, pp. 2391–2394, 2011.

[48] A. Silva-Juárez, C. J. Morales-Pérez, L. G. de la Fraga, E. Tlelo-Cuautle, and J. D. J. Rangel-Magdaleno, "On maximizing the positive Lyapunov exponent of chaotic oscillators applying DE and PSO," *Int. J. Dyn. Control*, vol. 7, no. 4, pp. 1157–1172, Sep. 2019.

[49] S. Wiggins, *Introduction to Applied Nonlinear Dynamical Systems and Chaos*. New York, NY, USA: Springer-Verlag, 2003.

[50] J. C. Sprott and A. Xiong, "Classifying and quantifying basins of attraction," *Chaos, Interdiscipl. J. Nonlinear Sci.*, vol. 25, no. 8, Aug. 2015, Art. no. 083101.

[51] V. H. Carbajal-Gomez, E. Tlelo-Cuautle, J. M. Muñoz-Pacheco, L. G. de la Fraga, C. Sanchez-Lopez, and F. V. Fernandez-Fernandez, "Optimization and CMOS design of chaotic oscillators robust to PVT variations: INVITED," *Integration*, vol. 65, pp. 32–42, Mar. 2019.

[52] R. Trejo-Guerra, E. Tlelo-Cuautle, J. M. Jiménez-Fuentes, C. Sánchez-López, J. M. Muñoz-Pacheco, G. Espinosa-Flores-Verdad, and J. M. Rocha-Pérez, "Integrated circuit generating 3- and 5-scroll attractors," *Commun. Nonlinear Sci. Numer. Simul.*, vol. 17, no. 11, pp. 4328–4335, Nov. 2012.

[53] E. Tlelo-Cuautle, J. J. Rangel-Magdaleno, A. D. Pano-Azucena, P. J. Obeso-Rodelo, and J. C. Nunez-Perez, "FPGA realization of multi-scroll chaotic oscillators," *Commun. Nonlinear Sci. Numer. Simul.*, vol. 27, nos. 1–3, pp. 66–80, Oct. 2015.

[54] A. D. Pano-Azucena, E. Tlelo-Cuautle, G. Rodriguez-Gomez, and L. G. de la Fraga, "FPGA-based implementation of chaotic oscillators by applying the numerical method based on trigonometric polynomials," *AIP Adv.*, vol. 8, no. 7, Jul. 2018, Art. no. 075217.

[55] V. Carbajal-Gomez, E. Tlelo-Cuautle, C. Sanchez-Lopez, and F. Fernandez-Fernandez, "PVT-robust CMOS programmable chaotic oscillator: Synchronization of two 7-scroll attractors," *Electronics*, vol. 7, no. 10, p. 252, Oct. 2018.

[56] O. Guillén-Fernández, A. Meléndez-Cano, E. Tlelo-Cuautle, J. C. Núñez-Pérez, and J. D. J. Rangel-Magdaleno, "On the synchronization techniques of chaotic oscillators and their FPGA-based implementation for secure image transmission," *PLoS ONE*, vol. 14, no. 2, Feb. 2019, Art. no. e0209618.

[57] J. M. Muñoz-Pacheco, E. Tlelo-Cuautle, I. Toxqui-Toxqui, C. Sánchez-López, and R. Trejo-Guerra, "Frequency limitations in generating multi-scroll chaotic attractors using CFOAs," *Int. J. Electron.*, vol. 101, no. 11, pp. 1559–1569, Jan. 2014.

[58] A. Buscarino, C. Corradino, L. Fortuna, M. Frasca, and J. C. Sprott, "Nonideal behavior of analog multipliers for chaos generation," *IEEE Trans. Circuits Syst. II, Exp. Briefs*, vol. 63, no. 4, pp. 396–400, Apr. 2016.

IRFAN AHMAD received the B.Sc. degree (Hons.) in electrical (telecommunication) engineering from Government College University Faisalabad, Faisalabad, Pakistan, in 2015, and the M.Sc. degree in electronics and communications engineering from Sirindhorn International Institute of Technology (SIIT), Thammasat University (TU), Thailand, in 2017, where he is currently pursuing the Ph.D. degree in electronics and communications engineering. He has been a Teaching and Research Assistant with SIIT. He has published articles, including IEEE Access. His research interests include chaos in higher dimensional circuits and systems, hidden oscillations, and chaos-based real-world applications. He was a recipient of the Excellent Foreign Student Scholarship from SIIT.

BANLUE SRISUCHINWONG received the B.Eng. degree (Hons.) from King Mongkut's Institute of Technology Ladkrabang, Bangkok, Thailand, in 1985, and the M.Sc. and Ph.D. degrees in electronics from The University of Manchester, U.K., in 1990 and 1992, respectively.

In 1987, he was a Research Assistant with Philips Research Laboratories, Eindhoven, The Netherlands. From 1992 to 1993, he was a Postdoctoral Research Associate with The University of Manchester. In 1993, he joined Sirindhorn International Institute of Technology (SIIT), Thammasat University (TU), Thailand. He was the Chair of the Department of Electrical Engineering, from 1993 to 1996, the Institute Secretary, from 2000 to 2002, and the Executive Assistant Director, from 2002 to 2007. He is currently an Associate Professor of electrical engineering. He has published five book chapters and over 90 articles, including IEEE Access, the IEEE Transactions on Instrumentation and Measurement, *Physics Letters A*, *Electronics Letters*, *Chaos, Solitons & Fractals* and the *International Journal of Circuit Theory and Applications*. His current research interests include chaos in circuits and systems, and nonlinear dynamics.

Dr. Srisuchinwong received the British Council Scholarship from U.K., from 1988 to 1991, and the Overseas Research Scholarship (ORS) Award from U.K., in 1988. He was a recipient of both the Excellent Research Publication Award and the Patent Award from SIIT, in 2019, and the Honor Plaque for a Merit from TU, in 2017. He won the Research Award from SIIT, in 2011, the Distinguished Research Award in Science and Technology from TU, in 2016, and the Best Paper Award from the Management and Innovation Technology International Conference, Thailand, in 2016. He was the Third Prize Winner of the ICT Award from the Ministry of Information and Communication Technology, Thailand, in 2010. He has served as a Reviewer for various reputable journals, including the IEEE Transactions on Circuits and Systems—II and the *Journal of the Franklin Institute*.